ORIGINAL ARTICLE

Consistency and prognostic value of preoperative staging and postoperative pathological staging using 18F-FDG PET/MRI in patients with non-small cell lung cancer

Akiko Kajiyama[1,2] · Kimiteru Ito[2] · Hirokazu Watanabe[2] · Sunao Mizumura[3] · Shun-ichi Watanabe[4] ·
Yasushi Yatabe[5] · Tatsuya Gomi[6] · Masahiko Kusumoto[2]

Abstract

Objective In recent years, positron emission tomography/magnetic resonance imaging (PET/MRI) has been clinically used as a method to diagnose non-small cell lung cancer (NSCLC). This study aimed to evaluate the concordance of staging and prognostic ability of NSCLC patients using thin-slice computed tomography (CT) and 18F-fluorodeoxyglucose (FDG) PET/MRI.

Methods This retrospective study was performed on consecutive NSCLC patients who underwent both diagnostic CT and 18F-FDG PET/MRI before surgery between November 2015 and May 2019. The cTNM staging yielded from PET/MRI was compared with CT and pathological staging, and concordance was investigated, defining pathological findings as reference. To assess the prognostic value of disease-free survival (DFS) and overall survival (OS), we dichotomized the typical prognostic factors and TNM classification staging (Stage I vs. Stage II or higher). Kaplan–Meier curves derived by the log-rank test were generated, and univariate and multivariate analyses were performed to identify the factors associated with DFS and OS.

Results A total of 82 subjects were included; PET/MRI staging was more consistent (59 of 82) with pathological staging than with CT staging. There was a total of 21 cases of CT and 11 cases of PET/MRI that were judged as cStage I, but were actually pStage II or pStage III. CT tended to judge pN1 or pN2 as cN0 compared to PET/MRI. There was a significant difference between NSCLC patients with Stage I and Stage II or higher by PET/MRI staging as well as prognosis prediction of DFS by pathological staging ($P < 0.001$). In univariate analysis, PET/MRI, CT, and pathological staging (Stage I or lower vs. Stage II or higher) all showed significant differences as prognostic factors of recurrence or metastases. In multivariate analysis, pathological staging was the only independent factor for recurrence ($P = 0.009$), and preoperative PET/MRI staging was a predictor of patient survival ($P = 0.013$).

Conclusions In NSCLC, pathologic staging was better at predicting recurrence, and preoperative PET/MRI staging was better at predicting survival. Preoperative staging by PET/MRI was superior to CT in diagnosing hilar and mediastinal lymph-node metastases, which contributed to the high concordance with pathologic staging.

Keywords Non-small cell lung cancer · 18F-FDG PET/MRI · CT · TNM staging · Prognosis

✉ Kimiteru Ito
kimito@ncc.go.jp

1 Department of Radiology, Toho University Graduate School of Medicine, Tokyo, Japan

2 Department of Diagnostic Radiology, National Cancer Center Hospital, 5-1-1 Tsukiji, Chuo-ku, Tokyo 104-0045, Japan

3 Department of Radiology, Toho University Omori Medical Center, Tokyo, Japan

4 Department of Thoracic Surgery, National Cancer Center Hospital, Tokyo, Japan

5 Department of Diagnostic Pathology, National Cancer Center Hospital, Tokyo, Japan

6 Department of Radiology, Toho University Ohashi Medical Center, Tokyo, Japan

Introduction

Lung cancer is the leading cause of cancer-related mortality in the world, and clinical imaging plays an important role in its diagnosis and management [1, 2], as the presence of the primary lung tumor and distant metastases influences therapy regimens and patient survival [3]. Computed tomography (CT) has been regarded as the standard method for the identification of pulmonary lesions [4]. For further scrutiny, ^{18}F-fluorodeoxyglucose (FDG) positron emission tomography (PET)/CT provides accurate data of lymph-node metastases [5]. However, frequent CT and PET/CT scans are disadvantageous for patients due to repeated radiation exposure [6]. This burden is increased at the time of preoperative examinations in particular, as both contrast-enhanced chest CT scan with breath-holding and whole-body CT without breath-holding accompanied by PET/CT are often performed. Magnetic resonance imaging (MRI) does not involve radiation exposure and has also been reported as one of the important proven methods to evaluate malignancies in pulmonary nodular diseases [7–11].

A combined PET/MRI machine has been newly released, and it has been used to detect various malignancies in clinical practice. A previous study comparing ^{18}F-FDG PET/MRI and ^{18}F-FDG PET/CT showed equivalent, high diagnostic performance for T and N staging in patients with non-small cell lung cancer (NSCLC) [12]. Several studies have also compared the diagnostic value of MRI with that of ^{18}F-FDG PET/CT in NSCLC patients and suggested that PET/MRI provides almost identical diagnostic ability as PET/CT without radiation exposure [3, 13]. However, the literature on the usefulness of clinical tumor staging by ^{18}F-FDG PET/MRI and its concordance with pathologic staging is currently unclear.

In this study, we retrospectively evaluated the concordance between clinical and pathologic staging and prognostic value of ^{18}F-FDG PET/MRI in preoperative NSCLC patients.

Materials and methods

Patients

Consecutive patients that were suspected to have lung cancer who received both CT and ^{18}F-FDG PET/MRI before surgery from November 2015 to May 2019 at National Cancer Center Hospital were enrolled in this study. The main purpose of the PET/MRI examination was to avoid radiation exposure while searching for lymph nodes and distant metastases other than the primary lung lesion and to exclude simultaneous second primary cancers in patients with preoperative lung cancer. The inclusion criteria were as follows: (1) pathologically proven non-small cell lung cancer, (2) both CT and PET/MRI were performed before thoracic surgery, and (3) follow-up after the operation was performed at the same institute. The exclusion criteria were as follows: (1) preoperative distant metastatic disease, (2) advanced primary cancer other than NSCLC, (3) treatment with chemotherapy before surgery, (4) multiple primary tumors, and (5) small nodular lesion less than 5 mm on the long axis by thin-slice CT images and/or PET/MRI. Since this was a retrospective single-center study, the informed consent requirement was waived by the institutional review board (research proposal number 2018–049).

^{18}F-FDG PET/MRI acquisition

Before the injection of ^{18}F-FDG, patients fasted for at least 4 h. If plasma glucose levels were less than 200 mg/dL, patients were injected intravenously with 3–4 MBq/kg of the radiotracer, depending on patient height and body weight. After injection, patients rested for 50–70 min before image acquisition. ^{18}F-FDG PET/MRI imaging was performed using a 3 T PET/MRI (SIGNA PET/MRI, GE Healthcare, Milwaukee, WI, USA). Patients were positioned in the supine headfirst position. The acquisition was started in the pelvic region and moved toward the head. The axial field of view contained the body volume from the head to the thigh. Both whole-body MRI and the adaptive PET/MRI images were reconstructed using time-of-flight ordered-subsets' expectation maximization (TOF-OSEM) with two iterations and 16 subsets and point spread function modeling, and 5.0 mm^3 post-filter at a dedicated workstation. The voxel size for whole-body PET was $3.125 \times 3.125 \times 2.780$ mm^3 (a matrix size of 192×192). After ensuring correct positioning of the spatial acquisition windows, the whole-body PET/MRI acquisition was initiated at a 2-min acquisition time per bed position. For attenuation correction of the PET data from the PET/MRI scanner, the reconstruction software provided by the manufacturer used attenuation maps generated based on the 3D two-point Dixon T1-weighted image obtained for every bed position. The procedure for MRI-based attenuation correction (MRAC) was implemented in the post-processing software of the scanner and operated automatically. The lungs were identified by connected component analysis of the air in the inner part of the body. By applying a morphologic closing filter, virtual air artifacts induced by the absence of an MRI signal in cortical bone, heart, and aorta (due to blood flow) were corrected. Attenuation of the PET signal caused by instrumentation, such as the patient bed and the fixed MRI coils, was automatically integrated into the

attenuation maps without contrast enhancement, at 5-mm slice thickness (axial and coronal) [14].

The MRI protocol comprised of the sequences in Table 1, which were acquired using PET. The whole-body PET/MRI protocol was performed using 16-channel upper and lower anterior array coils and a 16-channel central molecular imaging array coil. The adaptive PET/MRI protocol for the lung was performed using a 16-channel upper anterior array coil and a 16-channel central molecular imaging array coil. Intravenous contrast agents (meglumine gadoterate; Guerbet, Tokyo, Japan) were administered for contrast-enhanced T1-weighted images (ce-T1WI). The dose of contrast agent was adjusted from 0.1 to 0.2 ml/kg, up to a maximum dose of 15 ml, according to body weight and renal function. We most commonly performed ce-T1WI imaging of the chest and added ce-T1WI imaging of the brain if the clinician requested to examine brain metastases. A transversal diffusion-weighted (DWI) echo-planar imaging (EPI) sequence was performed using b values of 0 and 800 s/mm^2 in free breathing. After image acquisition, monoexponential ADC maps were calculated using the preinstalled software supplied by the vendor (GE health care, Milwaukee, WI, USA) on the associated PET/MRI console.

CT imaging

All CT scans of the study were performed on a multi-detector CT scanner (Aquilion PRIME, Aquilion Precision, Aquilion 64; Canon Medical Systems Corporation). Scans were performed supine after full inspiration with caudocranial scan direction including the entire ribcage and upper abdomen with tube-current modulation (range, 85–545 mA), and 120 kV. An intravenous contrast agent (iopamidol; Fuji-Pharma, Toyama, Japan) was used in most patients. The standard contrast agent dose was 520 mgI/kg, and imaging was started 80 s after contrast administration. Contiguous 5-mm section images were obtained and reconstruction of 1-mm thin-slice section images of the lung around the tumor was added.

All CT images were viewed using standard lung windows (window level, -600 HU; window width, 1900 HU). All image data were stored in DICOM format on PACS.

Image analysis

TNM staging was determined according to the UICC TNM Classification of Malignant Tumors, Eighth Edition. Location of primary tumors, tumor size in the greatest dimension, density of tumors, atelectasis, separate tumor nodules, and tumor invasion into the other structures were registered for clinical T-factor. Considering the quality of PET/MRI images, the size-criteria of T1 and T2 in the TNM classification were only defined as ≤ 3 cm and 3 cm to ≤ 5 cm,

Table 1 MR-sequence parameters

Category	Region	Orientation	Breathing motion	TR (ms)	TE (ms)	Scan time (sec)	Matrix size	Slice thickness (mm)	FOV (mm)	NEX	Flip angle
T1WI LAVA-FLEX	Whole body	Transverse	FB	4.4	TE_1 1.3 TE_2 2.6	13 s/bed	300×200	4	500×400	0.7	12°
T2WI single shot FSE	Whole body	Transverse	FB	1600	80	63 s/bed	384×224	6	500×500	0.5	90°
EPI-DWI	Thorax	Transverse	FB	10,000	72.7	160	160×140	5	350×320	5	90°
T2WI FSE sequence	Thorax	Transverse	BH	2250	102	36	320×192	5	350×250	1	111°
T2WI FSE sequence	Thorax	Coronal	BH	2200	102	36	320×192	5	350×350	1	111°
T1WI dual (in/opposed)	Thorax	Transverse	BH	150	TE_1 2.5 TE_2 5.8	36	320×192	5	350×280	1	60°
T1WI fast SPGR fat-sat CHESS (post-contrast)	Thorax	Coronal	BH	120	3.2	39	320×192	5	350×350	1	60°
T1WI LAVA-FLEX (post-contrast)	Thorax	Transverse	BH	6.7	1.4	16	300×192	5	350×280	0.7	12°

LAVA liver acquisition with volume acceleration, *FSE* fast spin echo, *EPI* echo-planar imaging, *DWI* diffusion-weighted image, *FB* free breathing, *BH* breath hold, *NEX* number of excitations, *SPGR* spoiled gradient recalled echo, *CHESS* chemical shift selective

respectively, and no subdivisions were used. Density criteria were assessed by only thin-slice CT alone and not by PET/MRI. Location of primary tumors, atelectasis, separate tumor nodules, and tumor invasion into other structures were assessed based on visual assessments of each modality.

One board-certified radiologist (HW) who specialized in chest imaging with 25 years of experience reviewed all chest CT images. Tumor size was assessed based on linear measurement of the largest diameter in axial thin-slice CT using lung windows. The reader used the monitor (Eizo RadiForce RX440) to measure the tumor size. The diagnosis of T3 was based on the thin-slice CT using mediastinal windows. In cases where the tumor diameter was less than 5 cm, infiltration was considered positive if the contact between the tumor and the parietal pleura was more than 3 cm, if there was thickening of the pleura in contact with the tumor, or if the tumor clearly formed a mass on the chest wall. In addition, nodular lesions were considered as intrapulmonary metastases if they were found in the same lobe by the thin-slice CT using lung windows, except for nodules with no change over time, or in cases with obvious calcification. For the diagnosis of N-factor, lymph-node metastasis was considered positive if the short diameter was 10 mm or more in thin-slice CT using mediastinal windows.

One nuclear medicine physician (KI), board-certified in diagnostic radiology with 16 years of experience, interpreted all PET/MRI images. An FDG–avid lesion was defined as focal, abnormally increased ^{18}F-FDG uptake versus background, with or without a corresponding anatomic lesion on the MR scan and suggestive of lung lesion and metastasis. PET/MRI images were analyzed using PET VCAR software by visually examining all the images on a computer display at the workstation (Advantage Workstation; GE Healthcare). The maximum standardized uptake value (SUVmax) of each lesion was measured visually using a sphere volume-of-interest. Tumor size was assessed by measuring the maximum diameter on the axial section of the MRI T2-weighted image. The sequence was selected based on previous studies [15, 16]. For the evaluation of the N-factor, involved lymph nodes were identified according to the following criteria: increased short-axis diameter (> 10 mm); central necrosis; lesions with distinct margin and round shape; visually high abnormal accumulation compared to surrounding tissue coincident with PET/MRI fusion image.

Pathological evaluation

Group of board-certified pathologists led by the chief pathologist specializing in lung cancer pathology (YY) reviewed hematoxylin–eosin stained, formalin-fixed paraffin-embedded specimens, histologically confirmed diagnosis, and evaluated histopathological findings of each case of lung cancer. Experienced pathologists aligned the cut surfaces of the resected specimen by referring to chest CT images.

Statistical analysis

Statistical analyses were performed using R [17]. Data were presented as mean ± standard deviation [SD], and a *P* value of 0.05 or less was considered significant. Fisher's exact test was performed to evaluate the agreement of PET/MRI and CT with pathology; κ statistics were performed to analyze the concordance of PET/MRI, CT, and pathological staging. Bland–Altman plots were used to examine the concordance of tumor size measurements performed based on PET/MRI, CT, and pathological specimens. For each type of measurement, the percentage of the relative difference between the tumor size measurements was plotted using the average of the two measurements. The limits of agreement were then calculated by taking the mean of the percentage of relative differences between the two measurements and two standard deviations of these differences.

Disease-free survival (DFS) was defined as the time from surgery until an occurrence of recurrence or metastasis or last follow-up visit. Overall survival (OS) was defined as the time from surgery to death from any cause or last follow-up. Surviving patients were censored at the last follow-up period. The last follow-up date for DFS and OS calculation was April 30, 2021. For DFS and OS analysis, the data were dichotomized by TNM staging (less than Stage I and higher than Stage II). DFS analysis of N-factor (N0 or higher than N1) was also performed. The log-rank (Mantel–Cox) test was used to evaluate the difference between Kaplan–Meier curves. To calculate the risk ratios and 95% confidence intervals (CIs), univariate analysis was used to identify factors associated with DFS and OS.

The factors were extracted based on previous studies [18–20], and those found to be significant by univariate analysis (*P* < 0.05) were entered into a Cox multivariate regression analysis model. For the univariate analysis, we used dummy variables of 1 for the following factors: age ≥ 75 y, male, ex-smoker or current smoker, and pathology other than squamous cell carcinoma. Then, forward stepwise multivariate regression analysis was performed to identify factors correlated with DFS and OS based on calculating hazard ratios (HRs) and 95% CIs.

Results

Patient characteristics

Two hundred fifty-four patients that were suspected of pulmonary malignancies and underwent both CT and PET/MRI were identified, and 82 patients that underwent lung
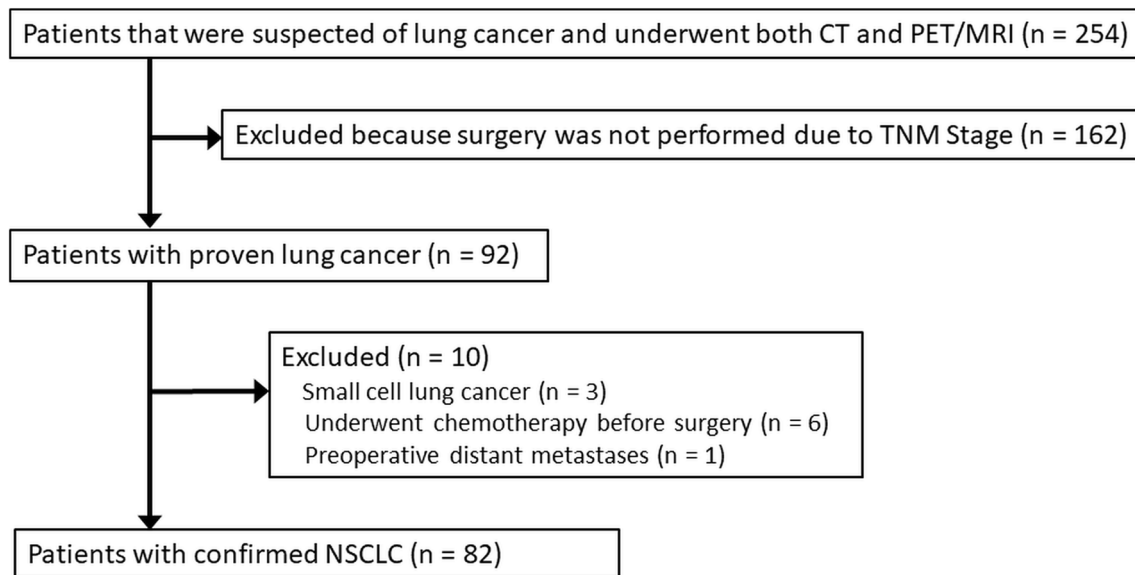
Fig. 1 Flow diagram of study patients

surgery and was pathologically confirmed as NSCLC were enrolled. A flow diagram summarizing the selection of patients is shown in Fig. 1. The majority of this cohort were men with adenocarcinoma who received lobectomy. Other clinical parameters are summarized in Table 2.

Characterization of imaging and pathological findings

The mean interval between PET/MRI and thin-slice CT was 1.9 ± 1.9 weeks. The mean interval between PET/MRI and operation was 3.1 ± 1.7 weeks, and between CT and operation was 3.7 ± 2.2 weeks. The median sizes of lung tumors identified by MRI, CT, and pathological specimens were 29 mm, 29 mm, and 32 mm, respectively.

The density of the tumors were as follows: one pure ground-glass nodule (GGN), 21 part-solid nodules, and 60 solid nodules.

The smallest solid nodule had a maximum diameter of 6 mm on MRI and a maximum CT diameter of 10 mm. The only pure GGN was measured to have a maximum diameter of 19 mm on MRI and a maximum diameter of 16 mm on CT.

Atelectasis of the peripheral lesion of the lung from the tumors was seen in one patient with a solid nodule. There was no patient with separate tumor nodules. Of the 82 cases, 21 were associated with withdrawn pleura, and 2 were suspected to have chest wall invasion.

The median value of SUVmax in the primary tumor was 7.84. A reference image of a case is shown in Fig. 2.

Correlation of imaging and pathology in tumor staging

Fisher's exact test showed no significant difference between PET/MRI and CT in terms of pathological staging or agreement with T- and N-factors ($P = 0.32$, $P = 0.52$, $P = 0.71$, respectively).

Table 3 shows the number of cases with concordant tumor staging for each modality: PET/MRI and pathology staging was concordant in 59/82 (72%) cases; CT and pathology and PET/MRI and CT staging were concordant in 52/82 (63%) and 65/82 (79%) cases, respectively. Of the cases judged to be cStage I by PET/MRI, 7 cases were actually pStage II and 4 cases were pStage III as determined by pathology. Of the cases judged to be cStage I by CT, 11 cases were actually pStage II and 10 cases were pStage III by pathology. Of the 11 cases that were understaged by PET/MRI, 3 cases that were judged cN0 were actually pN1 or pN2. Of the 21 understaged cases by CT, 11 cases that were judged cN0 were actually pN1 or pN2. A representative image showing the difference in N staging between PET/MRI and CT is shown in Fig. 3.

The kappa for PET/MRI and pathology staging and CT and pathology staging were 0.54 (95% CI 0.39–0.68, $P < 0.001$) and 0.36 (95% CI 0.21–0.51, $P < 0.001$), respectively; the kappa for PET/MRI and CT TNM staging was 0.59 (95% CI 0.43–0.75, $P < 0.001$).

Figure 4 shows the Bland–Altmann plot of tumor size measurement. Tumor size measurements presented by PET/MRI and CT were generally consistent (Fig. 4a), with a discrepancy between PET/MRI and pathology

Table 2 Patient characteristics ($n = 82$)

Characteristics		No. (%)
Age, years		
< 75		45 (54.9)
≥ 75		37 (45.1)
Sex		
Male		50 (61.0)
Female		32 (39.0)
Smoking status		
Never		23 (28.0)
Ex-smoker		55 (67.1)
Current smoker		4 (4.9)
Brinkman index		
< 400		34 (41.5)
≥ 400		48 (58.5)
Histology		
Adenocarcinoma		52 (63.4)
Squamous cell carcinoma		19 (23.2)
Large-cell carcinoma		3 (3.7)
Adenosquamous carcinoma		2 (2.4)
Invasive mucinous adenocarcinoma		2 (2.4)
Large-cell neuroendocrine carcinoma		2 (2.4)
Pleomorphic carcinoma		2 (2.4)
Operative method		
Segmentectomy		10 (12.2)
Lobectomy		66 (80.5)
Bilobectomy		3 (3.6)
Single lung total resection		3 (3.6)
Initial staging		
T	Total	82 (100)
Tis	Pathological	1 (1.2)
T1	PET/MRI clinical	48 (58.5)
	CT clinical	51 (62.1)
	Pathological	37 (45.1)
T2	PET/MRI clinical	27 (32.9)
	CT clinical	23 (28.0)
	Pathological	21 (25.6)
T3	PET/MRI clinical	3 (3.6)
	CT clinical	5 (6.0)
	Pathological	13 (15.8)
T4	PET/MRI clinical	4 (4.8)
	CT clinical	3 (3.6)
	Pathological	10 (12.1)
N	Total	82 (100)
N0	PET/MRI clinical	56 (68.2)
	CT clinical	69 (84.1)
	Pathological	58 (70.7)
N1	PET/MRI clinical	14 (17.0)
	CT clinical	8 (9.7)
	Pathological	14 (17.0)
N2	PET/MRI clinical	10 (12.1)
	CT clinical	4 (4.8)

Table 2 (continued)

		Initial staging	
		Pathological	9 (10.9)
N3		PET/MRI clinical	2 (2.4)
		CT clinical	1 (1.2)
		Pathological	0 (0)
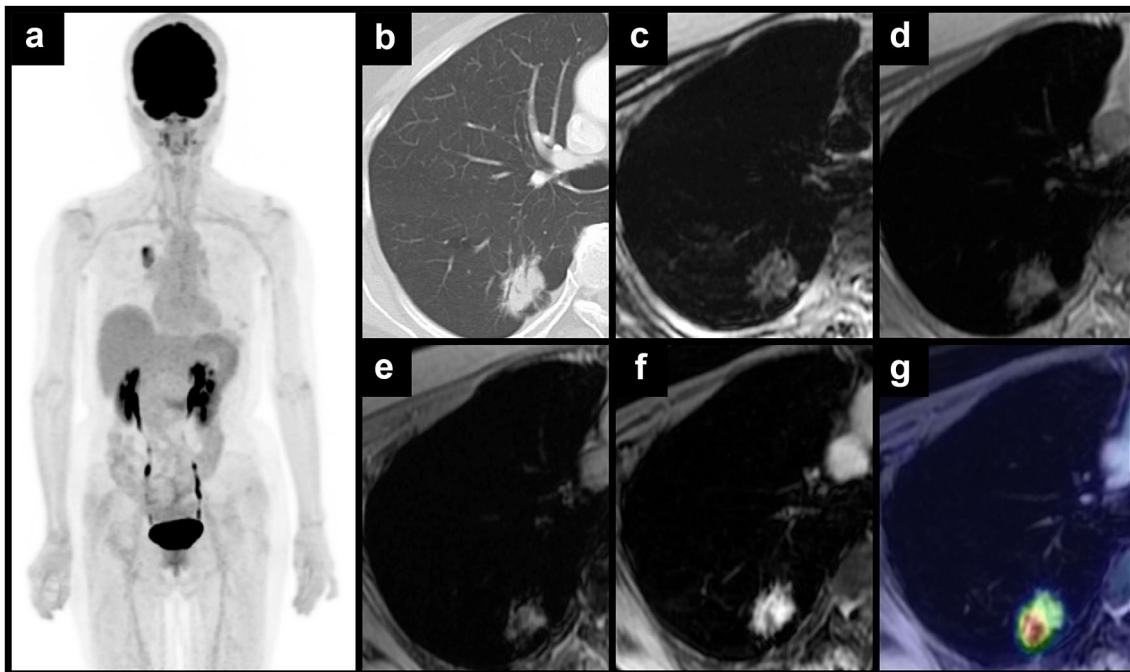
Fig. 2 CT and PET/MRI images of a 69-year-old woman. **a** PET/MRI maximum intensity projection image shows an accumulation on the right hilar side of the lung. **b** Axial thin-slice CT using lung windows image shows a pulmonary nodule in the lower lobe of the right lung. The same nodule is relatively clearly depicted on the following axial MRI images; **c** T2-weighted image, **d** in-phase T1-weighted image, **e** opposed-phase T1-weighted image, and **f** post-contrast water (fat-sat) T1-weighted image. **g** PET/MRI fusion images show high glucose uptake consistent with the nodule. The final diagnosis of this nodule was adenocarcinoma

tumor sizes of more than + 2 SD in 3 patients and -2 SD in 3 patients (Fig. 4b). Tumor size on CT and pathology deviated by more than + 2 SD in 1 patient and -2 SD in 4 patients (Fig. 4c). Two of the four patients with deviations of more than -2 SD on CT and pathology and one of the three patients with deviations of more than -2 SD on PET/MRI and pathology had severe emphysema. In cases where PET/MRI tumor diameter deviated from CT and pathologic tumor diameters, typical values of those with severe emphysema were 50 mm for PET/MRI, whereas it was 74 mm for CT and 78 mm for pathologic tumor. In the remaining two cases without associated emphysema, contractile changes with indrawn pleura were observed.

Patient outcome of survival

The mean follow-up term was 32.9 months (range: 5–62 months). Tumor recurrence and patient death were confirmed in 27 and 12 of 82 patients during the follow-up period, respectively. The Kaplan–Meier curve of DFS for each TNM stage evaluated by PET/MRI, CT, and pathology is shown in Fig. 5. The PET/MRI cStage I group showed a significantly better DFS rate than cStage II-III groups ($P < 0.001$), and the median DFS for cStage II–III groups was 17.54 months (Fig. 5a). Similarly, the groups of CT cStage I showed significantly better DFS rate than cStage II–IV groups ($P < 0.001$), and the median DFS for cStage II–IV groups was 17.54 months (Fig. 5b).

Table 3 Correlation between TNM staging methods

CT

PET/MRI	I	II	III	IV	Total
I	48	0	1	0	49
II	8	11	0	0	19
III	4	3	6	1	14
IV	0	0	0	0	0
Total	60	14	7	1	82

Pathology

PET/MRI	I	II	III	IV	Total
I	38	7	4	0	49
II	2	10	7	0	19
III	1	1	11	1	14
IV	0	0	0	0	0
Total	41	18	22	1	82

Pathology

CT	I	II	III	IV	Total
I	39	11	10	0	60
II	1	7	5	1	14
III	1	0	6	0	7
IV	0	0	1	0	1
Total	41	18	22	1	82
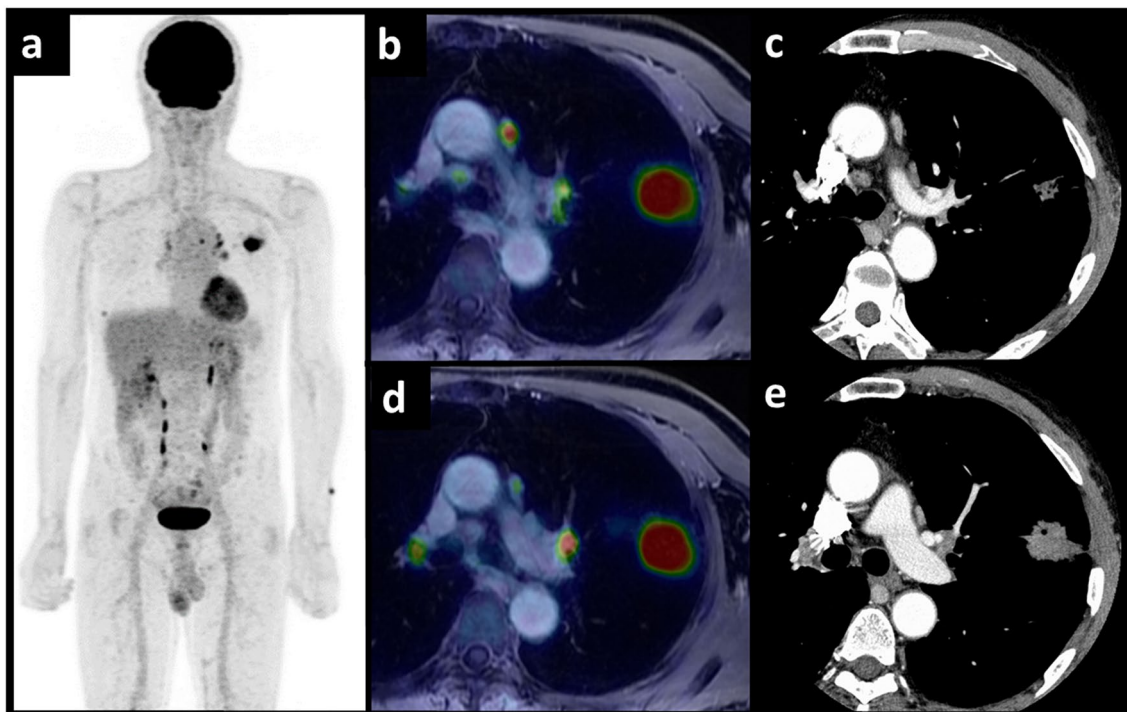
Fig. 3 PET/MRI and CT images of a 71-year-old man. **a** PET/MRI maximum intensity projection image shows an accumulation on the left lung and left mediastinal area. **b**, **d** PET/MRI fusion images show high glucose uptake consistent with primary lung tumor in the left lung, and in the left hilar and para-aortic lymph nodes. The tumor was diagnosed as cT2aN2 on PET/MRI. **c**, **e** Axial post-contrast thin-slice CT using mediastinal windows image shows the same tumor; however, the metastatic lymph nodes were not identified. The tumor was diagnosed as cT2aN0 in CT. After the operation, the pathological staging was pT3N2
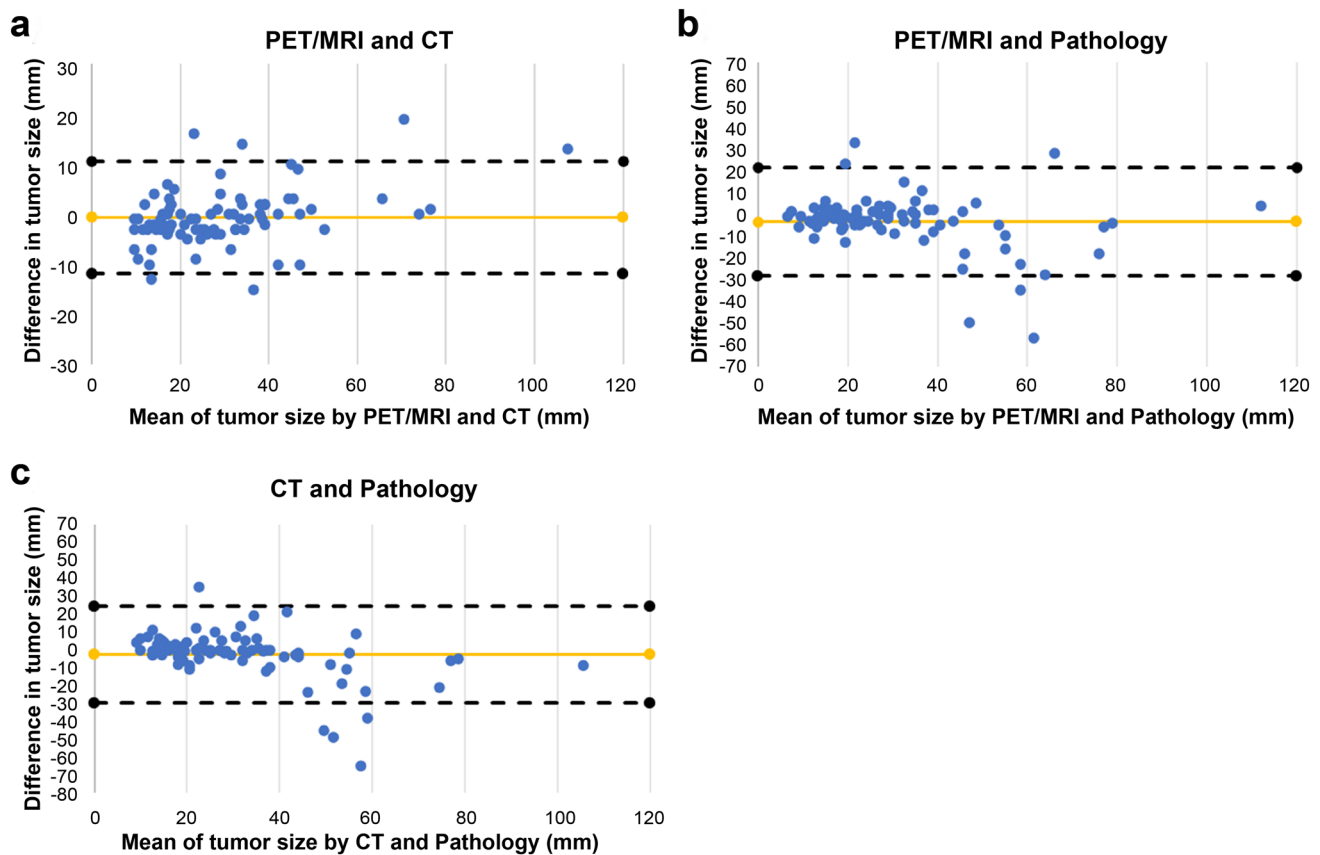
Fig. 4 Bland–Altman plots of ^{18}F-FDG PET/MRI and thin-slice CT and pathological specimen. Each figure shows lower and upper limits of agreement between **a** ^{18}F-FDG PET/MRI and thin-slice CT, **b** ^{18}F-FDG PET/MRI and pathological specimen, and **c** thin-slice CT and pathological specimen for primary tumor size (in mm). The difference between primary tumor sizes was plotted against the mean. **a** The mean difference between ^{18}F-FDG PET/MRI and thin-slice CT was − 0.63 mm (95% confidence interval: − 11.86; + 10.59). **b** The mean difference between ^{18}F-FDG PET/MRI and pathological specimen was − 3.43 mm (95% confidence interval: − 28.30; + 21.45). **c** The mean difference between thin-slice CT and pathological specimen was − 2.79 mm (95% confidence interval: − 29.89; + 24.31). No systematic bias was revealed by regression analysis

The median DFS for the group with pStage II–IV by pathological findings was 23.82 months, and the groups with pStage I or less showed significantly better DFS rate than pStage II–IV groups ($P < 0.001$) (Fig. 5c). In terms of OS, the group with Stage I or less by PET/MRI, CT, and pathological findings had significantly longer OS than the group with Stage II or higher ($P < 0.001$, $P = 0.03$, and $P = 0.01$, respectively).

For the N-factor, there was a significant difference in the Kaplan–Meier estimation of DFS for those judged to be cN0 vs. cN1-3 by PET/MRI ($P < 0.001$) (Fig. 5d).

Similarly, there was a significant difference in the Kaplan–Meier estimation of DFS for those judged to be cN0 vs. cN1-3 by CT and pN0 vs. pN1-2 by pathology ($P = 0.04$ and $P < 0.001$, respectively) (Fig. 5e, Fig. 5f).

The results of univariate and multivariate analysis of DFS are shown in Table 4. In univariate analysis, ^{18}F-FDG PET/MRI, CT, pathological staging, and SUVmax showed significant differences as factors. In multivariate analysis, only pathological staging remained as a predictor. For OS, PET/MRI staging showed a significant difference as a factor ($P = 0.013$), as shown in Table 5.

When N-factors derived from CT, PET/MRI, and pathology were included in univariate and multivariate analyses instead of Staging, only N-factor assessment of PET/MRI remained as a prognostic predictor of OS ($P = 0.004$).

Discussion

The findings of this study are twofold. First, preoperative staging by PET/MRI was more consistent with pathologic staging results than CT in NSCLC. Second, the prognosis of patients with NSCLC in Stage I and Stage II or higher categories was similar for PET/MRI and pathologic evaluation: only pathologic staging was a prognostic factor for DFS, whereas PET/MRI staging was a prognostic factor for OS.
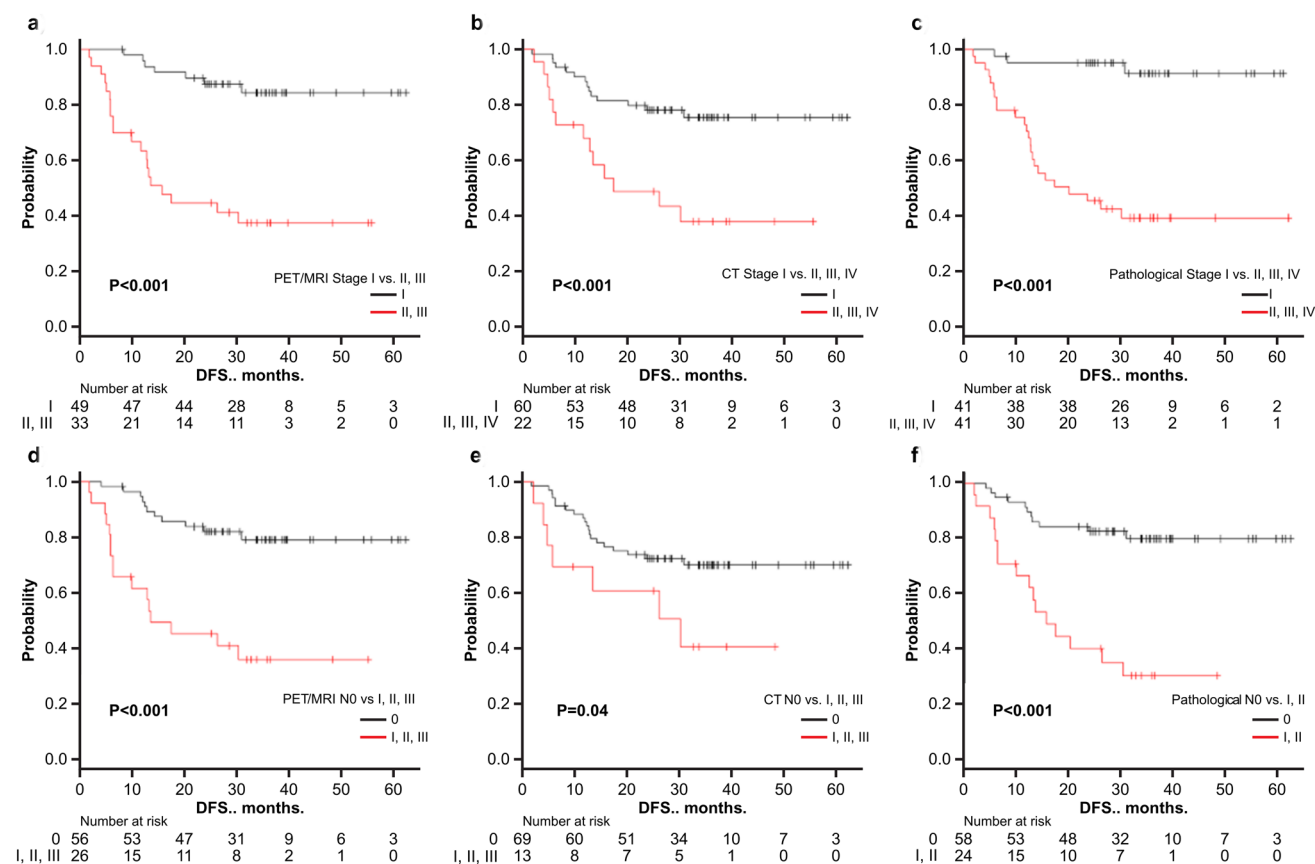
Fig. 5 Kaplan–Meier estimation of disease-free survival in NSCLC patients. The upper panel shows patients judged to be Stage I and Stage II or higher by PET/MRI (**a**), CT (**b**), and pathological staging (**c**). The lower panel shows patients classified as N0 and N1 or higher by PET/MRI (**d**), CT (**e**), and pathologically (**f**)

Lung tumor staging is defined by TNM factors, and in issuing the UICC Cancer Staging Manual 8th edition, the tumor diameter that defines the T-factor is subdivided compared to the 7th edition, indicating that the 8th edition of the T classification shows the importance of tumor density to predict patient prognosis [21, 22]. Thin-slice CT is considered to be the best modality for this evaluation. On the other hand, ^{18}F-FDG PET is generally not recommended for the evaluation of lung nodules smaller than 10 mm due to its spatial resolution. Pure GGNs can also result in a false-negative ^{18}F-FDG PET scan due to their low glucose metabolism [23, 24]. Furthermore, on chest MRI, lung nodules smaller than 5 mm are undetectable on T1WI or T2WI sequences [25, 26], and pure GGNs are also difficult to detect with routine MRI sequences. In this study, the smallest pulmonary nodule was calculated to be 10 mm in diameter by CT and 6 mm in diameter by MRI, although this was an incidental result, and there was only one case of pure GGN, which was 16 mm in diameter by CT and 19 mm in diameter by MRI. Therefore, small lung nodules and pure GGNs, which are difficult to detect by MRI as pointed out in the previous studies, could not be evaluated. These may be due to selection

bias by the clinicians who chose PET/MRI instead of PET/CT as part of the preoperative evaluation. Past literature comparing the size of lung cancer measured by preoperative CT with postoperative pathology reported that the size of the lung cancer measured by CT was significantly smaller in patients with emphysema than those without emphysema [27].

In the present study, advanced emphysema was confirmed in 2 of 4 patients with a deviation of -2 SD or more on Bland–Altmann plot on CT and in 1 of 3 patients on PET/MRI. Furthermore, the remaining two cases without associated emphysema both showed contractile changes with indrawn pleura and had a common histological type of lung adenocarcinoma. Park et al. reported that the pathologic tumor size of lung adenocarcinoma with indrawn pleura was significantly larger than the tumor size measured by CT compared to cases without indrawn pleura [28]. These results suggest that the images may underestimate the actual tumor size due to the influence of background lung and indrawn pleura.

Furthermore, PET/MRI and pathological staging agreed in 72% of cases, which was more consistent with

Table 4 Univariate and multivariate analyses of factors predictive of recurrence or metastases in patients

Variable	Hazard ratio	95% CI	P value
Univariate analysis			
PET/MRI stage			
≥ II	6.315	2.660–14.990	< 0.001*
< II	1	(reference)	
CT stage			
≥ II	3.316	1.556–7.070	0.002*
< II	1	(reference)	
Pathological stage			
≥ II	11.290	3.390–37.610	< 0.001*
< II	1	(reference)	
Pathology			
SCC	0.514	0.231–1.144	0.103
Non-SCC	1	(reference)	
Age			
≥ 75	0.812	0.327–2.011	0.652
< 75	1	(reference)	
Sex			
Female	0.900	0.417–1.940	0.788
Male	1	(reference)	
Smoking habit			
Ex- or current smoker	0.939	0.410–2.148	0.881
Non-smoker	1	(reference)	
SUVmax median value			
≥ 7.84	3.266	1.427–7.475	0.005*
< 7.84	1	(reference)	
Multivariate analysis			
PET/MRI stage			
≥ II	2.142	0.519–3.313	0.566
< II	1	(reference)	
CT stage			
≥ II	0.911	0.366–2.266	0.841
< II	1	(reference)	
Pathological stage			
≥ II	6.428	1.600–25.820	0.009*
< II	1	(reference)	
SUVmax median value			
≥ 7.84	1.547	0.579–4.139	0.385
< 7.84	1	(reference)	

CI confidence interval, *SCC* squamous cell carcinoma

Table 5 Univariate and multivariate analyses of factors predicting patient survival

Variable	Hazard ratio	95% CI	P value
Univariate analysis			
PET/MRI stage			
≥ II	10.87	2.424–48.700	0.002*
< II	1	(reference)	
CT stage			
≥ II	3.013	1.053–8.620	0.039*
< II	1	(reference)	
Pathological stage			
≥ II	4.257	1.213–15.650	0.024*
< II	1	(reference)	
Pathology			
SCC	0.3222	0.112–0.930	0.036*
Non-SCC	1	(reference)	
Age			
≥ 75	0.475	0.106–2.123	0.330
< 75	1	(reference)	
Sex			
Female	1.179	0.395–3.520	0.769
Male	1	(reference)	
Smoking habit			
Ex- or current smoker	5.265	0.688–40.280	0.110
Non-smoker	1	(reference)	
SUVmax median value			
≥ 7.84	3.142	0.980–10.070	0.054
< 7.84	1	(reference)	
Multivariate analysis			
PET/MRI stage			
≥ II	10.140	1.616–63.620	0.013*
< II	1	(reference)	
CT Stage			
≥ II	0.673	0.205–2.211	0.514
< II	1	(reference)	
Pathological stage			
≥ II	1.296	0.271–6.199	0.746
< II	1	(reference)	
Pathology			
SCC	0.603	0.200–1.817	0.369
Non-SCC	1	(reference)	

CI confidence interval, *SCC* squamous cell carcinoma

pathological staging results than CT (63%). The number of understaged cases was also lower with PET/MRI than with CT.

When we checked cases in which the tumor was understaged during CT and PET/MRI examinations compared to pathology, 21 cases were understaged by CT, of which 15 cases had discordant T-factors and 6 cases had discordant N-factors. On the other hand, 11 cases were understaged by PET/MRI, of which 8 cases had discordant T-factors and 3 cases had discordant N-factors. From the above, we considered the T-factor was more likely to be the cause of understaging.

In the evaluation of T-factors by PET/MRI, we did not add a special sequence for lung cancer as this was a retrospective study. In the past, some sequences have been modified to improve the evaluation of T-factors by PET/

MRI, but superiority over CT has still not been gained. [29].

Therefore, although the results of the present study indicate that PET/MRI and CT measurements may have less error in determining tumor size for NSCLC with tumor diameters of 5 mm or greater, the actual tumor size may be affected by background conditions, such as emphysema and pleural indentation. However, it is also clear that MRI with PET/MRI and low-dose CT with PET/CT are inferior to thin-slice CT in terms of density, so T-factor should still be evaluated with thin-slice CT, and ^{18}F-FDG PET/MRI should be used as a complement to thin-slice CT.

As for N-factors, CT had more cases in which pN1 and pN2 were judged as cN0 compared to PET/MRI. This may be due to the fact that CT could not detect hilar or mediastinal lymph-node metastases, for which PET/MRI was capable. On the other hand, for the T-factor, there was little difference between CT and PET/MRI, and the discrepancy between the results and pathology was due to the fact that the pleural infiltration detected by pathology could not be identified on the images.

Therefore, PET/MRI was superior to CT in diagnosing hilar and mediastinal lymph-node metastases, which may have contributed to the high concordance between PET/MRI and pathological staging. Meanwhile, the prognostic value of PET/MRI and pathology was similar in Stage I and II or higher categories. N-factor is one of the most important prognostic factors in determining patient survival from NSCLC [10]. Though there are size-criteria of 10 mm in diagnosing lymph-node involvement in conventional CT, this lower sensitivity than that of ^{18}F-FDG PET for focal lymph-node metastases can frequently occur in normal-sized nodes, and inflammation may also show irregular-sized nodes [3]. Therefore, ^{18}F-FDG PET/MRI is useful in N staging due to its detection of neoplasm of normal-sized lymph nodes by glucose metabolism and various MRI sequences [30–32]. The previous papers on the pathological N-factor of NSCLC using the 8th edition of the TNM classification state that there was a significant difference in OS between pN0 and pN1-3 regardless of the T-factor [33, 34]. Therefore, accurate determination of N-factor in operable patients is important from the viewpoint of prognosis between Stage I, which is based on N0M0, and Stage II and above, which involve factors N1-3. Furthermore, the DFS of N0 in this study was significantly longer than that of N1-3 classified by PET/MRI, and the results were similar to those of pathological N-factor classification. In addition, the prognostic value of NSCLC in the TNM Stage I group by PET/MRI, CT, and pathology showed significantly better prognosis than the Stage II group. Among them, pathological staging was an important predictor of recurrence in multivariate analysis, and only PET/MRI staging remained a factor when it came to predicting patient survival. And even after replacing the factor staging with N-factor, only N-factor by PET/MRI remained as a prognostic predictor of OS. Previous studies have reported that PET/CT is more predictive of OS in NSCLC patients compared to conventional imaging [35, 36], and these previous studies above and our results, combined with the fact that PET/MRI staging is more similar to pathological staging than CT and we speculate that the accuracy of PET/MRI assessment of N-factors may have influenced prognostic prediction.

Additionally, the following reasons were considered for why SUVmax did not contribute to prognosis in the present study. Several previous studies have reported that higher SUVmax is associated with a better prognosis in NSCLC, and the higher the SUVmax, the worse the prognosis. In reviewing the literature, those articles that reported SUVmax greater than 10 were more likely to report Stage II or higher patients [37, 38], and the papers reporting a significant difference in prognosis with low SUVmax (eg. SUVmax 5) seemed to be mostly for Stage I patients [39].

Although prognostic differences at low SUVmax 5 have also been reported [40], it included the patients after radiation therapy. Cerfolio et al. [41] reported a significant difference in prognosis in patients with SUVmax 10 and Stage IB or higher, but not in Stage IA patients. Therefore, it is possible that the literature that states that SUVmax is related to prognosis is characterized by a high number of patients with a high stage or a high SUVmax value dependent on the T-factor. From the above, we hypothesize that the reason why SUVmax did not contribute to prognosis in our study was that about half of the patients had Stage I disease, and the median SUVmax was lower than that in our study.

Although this study does not directly compare PET/CT and PET/MRI, there is a possibility that the use of preoperative PET/MRI in NSCLC patients may have an impact on patient outcomes in the future. In particular, the PET/MRI uses digital PET scanner with TOF reconstruction, which has improved resolution compared to older PET/CT scanners.

There are several limitations to this study. First, this study is a comparison between CT and PET/MRI and not PET/CT. Regarding to this point, the equivalence of diagnostic accuracy between PET/CT and PET/MRI has already been confirmed [42].

Furthermore, PET/MRI has a disadvantage due to its misalignment of images induced by the long breath-holds during the PET/MRI scan. However, except for very early stages, it is idealistic for most of the patients with lung cancer to receive baseline CE-brain MRI in addition to PET. And the drawback of MRI evaluation of lung regions can be partially compensated by the side-by-side reading of PET/MRI and thin-slice CT, which are always acquired before PET/MRI study. Moreover, as patients may receive multiple exposures by undergoing further PET/CT after CT imaging, we believe

that PET/MRI can be expected to serve as an alternative to PET/CT in the future from the perspective of radiation exposure. In addition, PET/MRI may also be used as an alternative when PET/CT cannot be reserved in daily practice.

Other factors include the retrospective design and relatively small patient population due to the selection of postoperative NSCLC patients who underwent both CT and PET/MRI.

Furthermore, there is no protocol for choosing PET/MRI instead of PET/CT preoperatively, and the decision was left up to the clinician, which may have created selection bias. Therefore, further prospective studies with a large number of patients are warranted. In addition, because of the recent introduction of PET/MRI at our institution, the observation period was short, averaging less than 5 years. Longer observation periods are needed to obtain solid evidence. Furthermore, although this study was conducted on patients with NSCLC who were eligible for surgery, the use of PET/MRI in patients who are not eligible for surgery or who have brain or bone metastases may help shorten the screening period, predict patient prognosis, and reduce patient radiation exposure. Finally, the high diagnostic accuracy of the N-factor in PET/MRI could be attributed to the relatively subjective nature of the PET/MRI reading, because it was performed by a single expert.

Conclusion

Preoperative staging by ^{18}F-FDG PET/MRI was superior to thin-slice CT in diagnosing hilar and mediastinal lymph-node metastases, which contributed to the high concordance with pathologic staging. Pathologic staging was a good predictor of recurrence in patients with NSCLC, and preoperative PET/MRI staging was a predictor of patient survival.

References

1. Molina JR, Yang P, Cassivi SD, Schild SE, Adjei AA. Non-small cell lung cancer: epidemiology, risk factors, treatment, and survivorship. Mayo Clin Proc. 2008;83(5):584–94.
2. Li F, Sher A, Kohan A, Vercher-Coonejero J, Rajiah P. PET/MRI in lung cancer. Semin Roentgenol. 2014;49(4):291–303.
3. Sawicki LM, Grueneisen J, Buchbender C, Schaarschmidt BM, Gomez B, Ruhlmann V, et al. Comparative performance of ^{18}F-FDG PET/MRI and ^{18}F-FDG PET/CT in detection and characterization of pulmonary lesions in 121 oncologic patients. J Nucl Med. 2016;57(4):582–6.
4. Lakshmanaprabu SK, Mohanty SN, Shankar K, Arunkumar N, Ramirez G. Optimal deep learning model for classification of lung cancer on CT images. Future Gener Comp Sy. 2019;92:374–82.
5. Yang W, Fu Z, Yu J, Yuan S, Zhang B, Li D, et al. Value of PET/CT versus enhanced CT for locoregional lymph nodes in non-small cell lung cancer. Lung Cancer. 2008;61(1):35–43.
6. Sodickson A, Baeyens PF, Andriole KP, Prevedello LM, Nawfel RD, Hnason R, et al. Recurrent CT, cumulative radiation exposure, and associated radiation-induced cancer risks from CT of adults. Radiology. 2009;251(1):175–84.
7. Yi CA, Shin KM, Lee KS, Kim BT, Kim H, Kwon OJ, et al. Non-small cell lung cancer staging: efficacy comparison of integrated PET/CT versus 3.0-T whole-body MR imaging. Radiology. 2008;248(2):632–42.
8. Sommer G, Koenigkam-Santos M, Biederer J, Puderbach M. Role of MRI for detection and characterization of pulmonary nodules. Radiology. 2014;54(5):470–7.
9. Plathow C, Aschoff P, Lichy MP, Eschmann S, Heur T, Brink I, et al. Positron emission tomography/computed tomography and whole-body magnetic resonance imaging in staging of advanced nonsmall cell lung cancer-initial results. Invest Radiol. 2008;43(5):290–7.
10. Heusch P, Buchbender C, Kohler J, Nensa F, Gauler T, Gomez B, et al. Thoracic staging in lung cancer: prospective comparison of 18F-FDG PET/MR imaging and 18F-FDG PET/CT. J Nucl Med. 2014;55(3):373–8.
11. Lee SM, Goo JM, Park CM, Yoon SH, Paeng JC, Cheon GJ, et al. Preoperative staging of non-small cell lung cancer: prospective comparison of PET/MR and PET/CT. Eur Radiol. 2016;26(11):3850–7.
12. Kirchner J, Sawicki LM, Nensa F, Schaarschmidt BM, Reis H, Ingenwerth M, et al. Prospective comparison of ^{18}F-FDG PET/MRI and ^{18}F-FDG PET/CT for thoracic staging of non-small cell lung cancer. Eur J Nucl Med Mol Imaging. 2019;46(2):437–45.
13. Schaarschmidt BM, Grueneisen J, Metzenmacher M, Gomez B, Gauler T, Roesel C, et al. Thoracic staging with ^{18}F-FDG PET/MR in non-small cell lung cancer - does it change therapeutic decisions in comparison to ^{18}F-FDG PET/CT? Eur Radiol. 2017;27(2):681–8.
14. Delso G, Martinez-Möller A, Bundschuh RA, Ladebeck R, Candidus Y, Faul D, et al. Evaluation of the attenuation properties of MR equipment for its use in a whole-body PET/MR scanner. Phys Med Biol. 2010;55(15):4361–74.
15. Messerli M, Barbosa FDG, Marcon M, Muehlematter UJ, Stolzmann P, Warschkow R, et al. Value of PET/MRI for assessing tumor resectability in NSCLC-intra-individual comparison with PET/CT. Br J Radiol. 2018;92:20180379.
16. Fleichsig P, Mehndiratta A, Haberkorn U, Kratochwil C, Giesel FL. PET/MRI and PET/CT in lung lesions and thoracic malignancies. Semin Nucl Med. 2015;45:268–81.
17. Kanda Y. Investigation of the freely available easy-to-use software 'EZR' for medical statistics. Bone Marrow Transplant. 2013;48(3):452–8.
18. Chansky K, Sculier JP, Crowley JJ, Giroux D, Meerbeeck JV, Goldstraw P. The international association for the study of lung cancer staging project prognostic factors and pathologic TNM stage in surgically managed non-small cell lung cancer. J Thorac Oncol. 2009;4(7):792–801.
19. Sculier JP, Chansky K, Crowley JJ, Meerbeeck JV, Goldstraw P. The impact of additional prognostic factors on survival and their relationship with the anatomical extent of disease as expressed by the 6th edition of the TNM classification of malignant tumours and the proposals for the 7th edition. J Thorac Oncol. 2008;3(5):457–66.
20. Berghmans T, Dusart M, Paesmans M, Hossein-Foucher C, Buvat I, Castaigne C, et al. Primary tumor standardized uptake value (SUV$_{max}$) measured on fluorodeoxyglucose positron emission tomography (FDG-PET) is of prognostic value for survival in non-small cell lung cancer (NSCLC): a systematic review and meta-analysis (MA) by the European lung cancer working party for the IASLC lung cancer staging project. J Thorac Oncol. 2008;3(1):6–12.

21. Lim W, Ridge CA, Nicholson AG, Quant SM. The 8th lung cancer TNM classification and clinical staging system: review of the changes and clinical implications. Quant Imaging Med Surg. 2018;8(7):709–18.

22. Rami-Porta R, Bolejack V, Crowley J, Ball D, Kim J, Lyons G, et al. The IASLC lung cancer staging project: proposals for the revisions of the T descriptors in the forthcoming eight edition of the TNM classification for lung cancer. J Thorac Oncol. 2015;10(7):990–1003.

23. Nomori H, Ohba Y, Yoshimoto K, Shibata H, Shiraishi K, Mori T. Positron emission tomography in lung cancer. Gen Thorac Cardiovasc Surg. 2009;57(4):184–91.

24. Iwano S, Ito S, Tsuchiya K, Kato K, Naganawa S. What causes false-negative PET findings for solid-type lung cancer? Lung Cancer. 2013;79(2):132–6.

25. Biederer J, Schoene A, Freitag S, Reuter M, Heller M. Simulated pulmonary nodules implanted in a dedicated porcine chest phantom: sensitivity of MR imaging for detection. Radiology. 2003;227(2):475–83.

26. Koyama H, Ohno Y, Kono A, Takenaka D, Maniwa Y, Nishimura Y, et al. Quantitative and qualitative assessment of non-contrast-enhanced pulmonary MR imaging for management of pulmonary nodules in 161 subjects. Eur Radiol. 2008;18(10):2120–31.

27. Sugawara H, Watanabe H, Kunimatsu A, Abe O, Yatabe Y, Watanabe S, et al. Tumor size in patients with severe pulmonary emphysema might be underestimated on preoperative CT. Eur Radiol. 2022;32(1):163–73.

28. Park CH, Kim TH, Lee S, Moon DH, Park HS. Correlation between maximal tumor diameter of fresh pathology specimens and computed tomography images in lung adenocarcinoma. PLoS ONE. 2019;14(1):1–13.

29. Dahlsgaard-Wallenius SE, Hildebrandt MG, Johansen A, Vilstrup MH, Petersen H, Gerke O, et al. Hybrid PET/MRI in non-small cell lung cancer (NSCLC) and lung nodules—a literature review. Eur J Nucl Med Mol Imaging. 2021;48:584–91.

30. Wiener JI, Chako AC, Merten CW, Gross S, Coffey EL, Stein HL. Breast and axillary tissue MR imaging: correlation of signal intensities and relaxation times with pathologic findings. Radiology. 1986;160(2):299–305.

31. Ohno Y, Hatabu H, Takenaka D, Higashino T, Watanabe H, Ohbayashi C, et al. Metastases in mediastinal and hilar lymph nodes in patients with non-small cell lung cancer: quantitative and qualitative assessment with STIR turbo spin-echo MR imaging. Radiology. 2004;231(3):872–9.

32. Ohno Y, Koyama H, Yoshikawa T, Nishio M, Aoyama N, Onishi Y, et al. N stage disease in patients with non–small cell lung cancer: efficacy of quantitative and qualitative assessment with STIR turbo spin-echo imaging, diffusion-weighted MR imaging, and fluorodeoxyglucose PET/CT. Radiology. 2011;261(2):605–15.

33. Katsumata S, Aokage K, Ishii G, Nakasone S, Sakai T, Okada S, et al. Prognostic impact of the number of metastatic lymph nodes on the eighth edition of the TNM classification of NSCLC. J Thorac Oncol. 2019;14(8):1408–18.

34. Shang X, Liu J, Li Z, Lin J, Wang H. A hypothesized TNM staging system based on the number and location of positive lymph nodes may better reflect the prognosis for patients with NSCLC. BMC Cancer. 2019;19(1):591.

35. Antoniou AJ, Marcus C, Tahari AK, Wahl RL, Subramaniam RM. Follow-up or surveillance ^{18}F-FDG PET/CT and survival outcome in lung cancer patients. J Nucl Med. 2014;55(7):1062–8.

36. Gregory DL, Hicks RJ, Hogg A, Binns DS, Shum PL, Milner A, et al. Effect of PET/CT on management of patients with non–small cell lung cancer: results of a prospective study with 5-year survival data. J Nucl Med. 2012;53(7):1007–15.

37. Ahuja V, Coleman RE, Herndon J, Patz EF Jr. The prognostic significance of fluorodeoxyglucose positron emission tomography imaging for patients with nonsmall cell lung carcinoma. Cancer. 1998;83:918–24.

38. Eschmann SM, Friedel G, Paulsen F, Reimold M, Hehr T, Budach W, et al. Is standardised 18F-FDG uptake value an outcome predictor in patients with stage III non-small. Eur J Nucl Med Mol Imaging. 2006;33:263–9.

39. Higashi K, Ueda Y, Arisaka Y, Sakuma T, Nambu Y, Oguchi M, et al. 18F-FDG uptake as a biologic prognostic factor for recurrence in patients with surgically resected. J Nucl Med. 2002;43(1):39–45.

40. Sasaki R, Komaki R, Macapinlac H, Erasmus J, Allen P, Forster K, et al. [18F] fluorodeoxyglucose uptake by positron emission tomography predicts outcome of non-small-cell lung cancer. J Clin Oncol. 2005;23(6):1136–43.

41. Cerfolio RJ, Bryant AS, Ohja B, Bartolucci AA. The maximum standardized uptake values on positron emission tomography of a non-small cell. J Thorac Cardiovasc Surg. 2005;130(1):151–9.

42. Spick C, Herrmann K, Czernin J. 18F-FDG PET/CT and PET/MRI perform equally well in cancer: evidence from studies on more than 2300 patients. J Nucl Med. 2016;57(3):420–30.